Improving pose estimation accuracy and expanding of visible space of lighting 3D marker in turbid water

1st Horng-Yi Hsu
Graduate school of Natural Science and Technology, Okayama University
Okayama, Japan
pcvv4h2h@s.okayama-u.ac.jp

2nd Naoki Mukada
Graduate school of Natural Science and Technology, Okayama University
Okayama, Japan
pola9zud@s.okayama-u.ac.jp

3rd Daiki Yamada
Graduate school of Natural Science and Technology, Okayama University
Okayama, Japan
p7kw2h27@s.okayama-u.ac.jp

4th Khin Nwe Lwin
University of Technology
Yangon, Myanmar
knlwin85@gmail.com

5th Myo Myint
Thanlyin Technological University
Thanlyin, Myanmar
ecmyomyint@gmail.com

6th Yuichiro Toda
Graduate school of Natural Science and Technology, Okayama University
Okayama, Japan
ytoda@okayama-u.ac.jp

7th Takayuki Matsuno
Graduate school of Natural Science and Technology, Okayama University
Okayama, Japan
matsuno@cc.okayama-u.ac.jp

8th Keigo Watanabe
Graduate school of Natural Science and Technology, Okayama University
Okayama, Japan
watanabe@sys.okayama-u.ac.jp

9th Mamoru Minami
Graduate school of Natural Science and Technology, Okayama University
Okayama, Japan
minami-m@cc.okayama-u.ac.jp

***Abstract*—Aiming at developing underwater battery recharging system, the author developed a docking system using stereo-vision-based visual servoing and a 3D marker. The 3D marker consists of red, green, blue spheres that do not emit the light which is named as a passive marker. Real-time relative pose (position and orientation) estimation was implemented utilizing the 3D model-based matching method and real-time multi-step genetic algorithm (RM-GA). Given the situation that the docking aims for battery recharging in the deep-sea bottom, the pitch-dark and turbid environment should be considered as an inevitable condition for battery recharging. In our previous works, the docking experiments were conducted in the actual sea, having verified the effectiveness of the proposed system using the passive 3D marker in the daytime environment with turbid water condition. Since lighting passive 3D marker by light from the vehicle in turbid water environment results in a situation that the images taken by video cameras set on the vehicle were looked wholly white, some new idea seems to be required. To overcome this difficulty, the newly lighting 3D marker (active 3D maker) has LEDs inside was introduced in the previous work. The main objective of this study is to check the feasibility area of the proposed system for the docking application, comparison of recognition performance using the active and passive 3D marker that was conducted in the simulated pool with the turbid water is focused. And then, the experiment using the active 3D marker in the actual sea has been performed. The experimental results have confirmed that the new active 3D marker with no-lighting from the vehicle could be recognizable in dark and turbid environment than the passive 3D marker with the lighting from the vehicle.**

***Index Terms*—Dual-eye, Visual servoing, Turbidity, Recognition, 3D marker**

I. Introduction

In recent years, various underwater robots have been researched and developed for seabed exploration, submarine mapping, an ecological survey of underwater organisms, mining of underground resources and so on. To do this kind of works, the underwater robots need to be active for a long time in the seabed. The two main ways of supplying power to the robot are wired and battery. In the case of ROV (Remotely Operated Vehicle), the cable is liable to be damaged due to contact with rocks at the seabed. Also, the cable will be several thousand meters long in order to dive into the deep-sea. In the case of AUV (Autonomous Underwater Vehicle), the power capacity of the battery that is attached to the vehicle is one of the main limitations when the operations take longer than the duration supported by the battery of the vehicle. The vehicle is necessary to move back and forth between the ship from the surface and the workplace of the seabed for battery charging. Therefore, decreasing the working time and efficiency in the deep-sea became the problems for the deep-sea applications. To overcome this problem and prolong the activity time in the seabed, an underwater recharging station with a docking function has been researched in the seabed using different kinds of approach.

There are many studies on underwater docking using different approaches. Depending on a docking station's structure for a specific application, different methods and sensors were utilized. Homing accuracy and robustness against disturbances are critical requirements for docking operation. To fulfill these demands, many studies have been conducted recently. Among them, it is roughly divided into a method using monocular camera [1] and stereo camera [2] for homing and docking. Docking was conducted for the submersible power supply with an ultrasonic sensor and monocular camera with the control error of $\pm$100 mm [3].

In contrast, a vision-based docking system using two cameras and a 3D marker has been developed by our research group. In previous works, we especially confirmed the performance of 3D pose estimation and visual servoing, which are one of the docking steps in our approach using real-time pose estimation. In [4], real-time pose tracking ability with stereo-vision was confirmed when a target was moving even though there were some noise in captured images due to air bubbles in front of the cameras. In that paper not only noise disturbances in images but also physical disturbances of water stream induced by floating motion of air bubbles were given to the ROV, having confirmed whether the proposed approach is robust enough to be able to operate in the actual sea. In [5], 3D pose estimation with partial occlusion was discussed. In [6], docking procedure was implemented and docking experiment was conducted when the ROV's starting positions were given arbitrarily in front of the 3D marker. As a follow-up work, we also checked the robustness of our system under a varying light environment in [7]. In [8], the sea docking experiment using a circular shaped docking hole was reported. Since this experiment was conducted in a relatively transparent sea in a part of the harbor, measurement of 3D marker for estimating the pose of ROV was successful.

In such a wide range of actual seabed, the vision-based vehicles have to face the difficulty for the recognition because the proliferation of mud will cause poor visibility by the thrust of the underwater robot and other disturbances such fish, seaweed, turbidity, lighting changing, and so on. The vehicle cannot avoid the turbidity and dark environment for the sea bottom battery recharging. According to the authors' knowledge, there are no studies using stereo-vision and 3D marker for real-time visual servoing with the performance of turbidity tolerance and illumination varieties. In our previous works, docking experiments were conducted against turbidity and changing lighting environment. In [9], the performance of the 3D pose estimation system under different turbidity levels was analyzed by using 3D marker, and the turbidity tolerance of the system was examined experimentally.

In the case of using the 3D marker, the ROV's lighting was used to detect the 3D marker in the dark environment. Since lighting 3D marker by light from vehicles in turbid water environment results in the images was looked wholly white. To overcome this problem, the active marker was designed and constructed to improve the 3D pose estimation system against turbid and dark environment. In [10], the robustness of the proposed docking approach was verified in a simulated pool under changing lighting condition. The practicality of the proposed system was confirmed by conducting the sea docking experiment against turbidity. In here, even though the active marker was used to improve the 3D pose estimation system, we did not compare the turbidity tolerance by using active and passive 3D marker against turbidity. In the present study, recognition performances using active and passive 3D marker are compared, having confirmed that the new active 3D marker with no-lighting from the vehicle could be more recognizable in dark and turbid environment than the passive 3D marker lighted from the vehicle.

The recognition experiments were conducted by simulating a turbid environment in the experimental pool using the active and passive 3D marker. The turbidity levels and the distance between the active/passive 3D marker and ROV were varied as variables, and the recognizable range of the active/passive 3D marker was confirmed by RM-GA. The recognition experiment consists of two ways (1) A method of recognizing passive 3D marker using LED illumination mounted on ROV, and (2) A method of recognizing active 3D marker without LED illumination mounted on the ROV. According to the experimental results, it can be known that the ability of using the active 3D marker compared with using the passive 3D marker, both the recognizable distance and the recognizable turbidity level have increased.

II. Active 3D Marker

The illustration of light transmission using passive and active 3D marker in pitch-dark and the turbid environment shown in Fig. 1. Figure 1(a) shows the light transmission of the passive marker lighted by the ROV‘s LED lighting. Figure 1(b) shows the light transmission, when the active marker illuminates by itself and ROV‘s cameras receive the light. In the case of using the passive 3D marker, light is reflected, scattered and attenuated, results in whiteout. In the case of using the active 3D marker, light reaches ROV‘s cameras directly. Since the cameras cannot photograph the reflected light in impure water, it is considered that active 3D marker will be photographed more clearly. In the turbid environment, the camera images of the active 3D marker have become unclear images in the outline of the marker sphere. So that, the pose estimation accuracy may be deteriorated.

Therefore, red, green, and blue LEDs are built in each sphere of the active 3D marker. When light of each color is emitted, light reaches directly to the ROV cameras as shown in Fig. 1 (b). Also, the distance of light passes in (b) is half of (a). It is thought that it is less likely to be affected by turbidity.

III. Fitness Function

In this experiment, a fitness value is used to evaluate the performance of the recognition under different turbidity levels and distance. A correlation function of the real target projected in camera images with the assumed model, represented by poses in the chromosomes, is used as the fitness function in the GA process. Fitness function has been modified based on the voting performance and the target's structure (color, size, and shape). The fitness function is defined as the following equation (1), where ϕ means position and posture of 3D

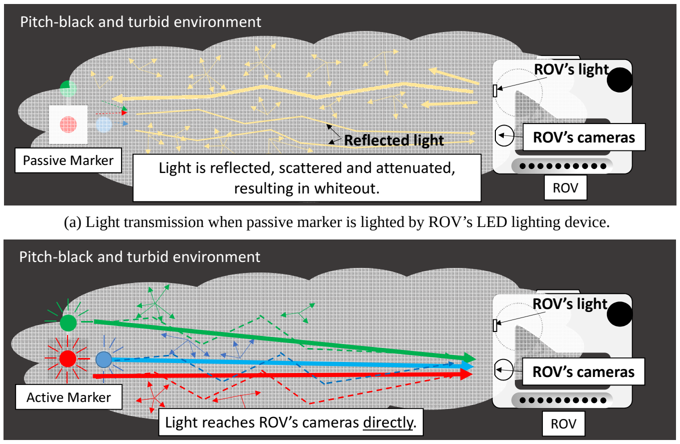

(a) Light transmission when passive marker is lighted by ROV's LED lighting device.

(b) Light transmission when active marker illuminates by itself and ROV's cameras receive the light.

Fig. 1. Illustration of light transmittion using passive and active marker in pitch-dark and turbid environment.

marker that relative to the fixed coordinate system of the ROV. The evaluation function that is used for ϕ and the image taken by cameras is defined by the previous research [11]. ϕ_i means pose of the i-th model that was given by the RM-GA.

The left or right image of the solid 3D model to estimate the pose of the real 3D marker is shown in Fig. 2. This solid 3D model is made from the point cloud that made from the color and shape of 3D marker. The fitness calculation of equation (1) is described as below. In Fig. 2, fitness value is calculated by evaluating the inner sphere S_{in} overlap the hue value of the image. The function $p\left({}^{IL}\mathbf{r}_j\left(\phi_i\right)\right)$ is a function that gives a score "1" when the j-th model ${}^{IL}\mathbf{r}_j\left(\phi_i\right)$ of the point group of the model determined by the i-th candidate ϕ_i of the pose overlaps with the active 3D marker.

$$F\left(\phi_i\right) = \frac{1}{2}\left(F_L + F_R\right)$$

$$F_L = \frac{1}{N}\left(\sum_{{}^{IL}\mathbf{r}_j(\phi_i)\in S_{L,in}(\phi_i)} p\left({}^{IL}\mathbf{r}_j\left(\phi_i\right)\right) + \sum_{{}^{IL}\mathbf{r}_j(\phi_i)\in S_{L,out}(\phi_i)} p\left({}^{IL}\mathbf{r}_j\left(\phi_i\right)\right)\right)$$

$$F_R = \frac{1}{N}\left(\sum_{{}^{IR}\mathbf{r}_j(\phi_i)\in S_{R,in}(\phi_i)} p\left({}^{IR}\mathbf{r}_j\left(\phi_i\right)\right) + \sum_{{}^{IR}\mathbf{r}_j(\phi_i)\in S_{R,out}(\phi_i)} p\left({}^{IR}\mathbf{r}_j\left(\phi_i\right)\right)\right) \quad (1)$$

Similarly, the evaluation of the fitness value is calculated for the enveloping sphere S_{out} of the search model. The inner sphere of the red model S_{in} is intended to evaluate the red ball area of the real target, and the enveloping sphere S_{out} is for the background area.The fitness function is calculated by averaging the fitness functions of both the left camera image F_L and right camera image F_R. The summation in (1) is concerning the jth point ${}^{IL}\mathbf{r}_j\left(\phi_i\right)$, defined on the ith 3-D model, whose pose is ϕ_i . In (1), N represents the number of jth points, where $j = 1, 2, ..., N$. The calculation of fitness value is averaged over the left and right camera images to obtain the final fitness value $F\left(\phi_i\right)$ consists of pose information[x [mm], y [mm], z [mm], ε_1, ε_2, ε_3] (ε_1, ε_2, ε_3 are quaternions).

The 3D model was created by using the information of the ith candidate pose ϕ_i is projected to the left and right camera images, and the correlation with the active 3D marker is evaluated as the fitness value. The entered left and right camera images are used for evaluation without performing image processing. The search model matches the 3D marker when the relationship between various parameters of the camera and kinematics is perfectly matched and the search model accurately represents the shape of the recognition object. At this time, $F\left(\phi_i\right)$ is configured to take the maximum value, and the pose ϕ_i of the search model giving the maximum value represents the pose of the 3D marker.

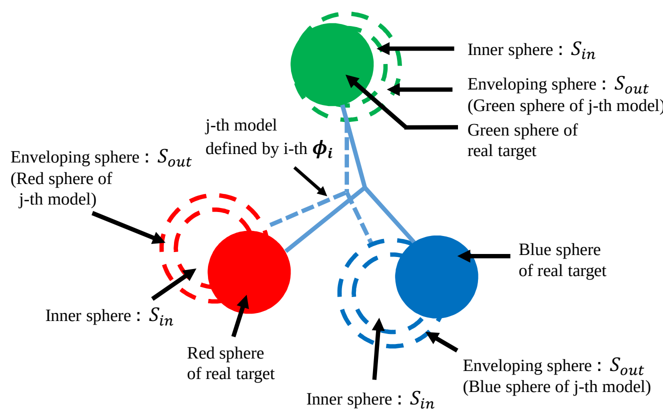

Fig. 2. Left or right camera's 2D image of the real 3D marker and model

IV. Comparison Experiment of Recognition Performance That Using Active and Passive 3D Marker

For comparing recognize capabilities by the conditions of using two kinds of 3D marker, the recognition experiments have been performed. The recognition experiments are conducted in the simulated pool.

A. Experiment Environment

The experimental layout of the recognition experiments is shown in Fig. 3. Figure 3 shows the experiment environment using active 3D marker and coordinate system of the ROV and 3D marker. $\sum_H$ and $\sum_M$ are the coordinate system of the ROV and passive 3D marker. The defined coordinate system of the experiment by using passive 3D marker is same as the experiment by using active 3D marker. The ROV is fixed in the pool so that the pose between the ROV and the 3D marker is kept constant. Recognition distance is set to 400, 600, 800 and 1000 mm.

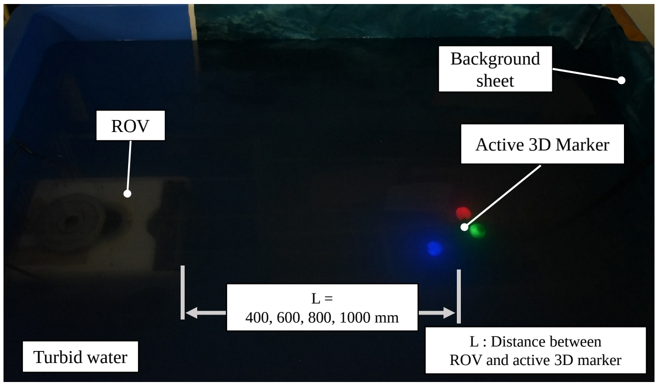

Fig. 3. Experimental environment using active marker. Photograph of ROV and active marker in dark environment.

B. Turbidity Environment

The turbidity environment is created by putting milk in the simulated pool. According to the other researchs [12], [13], there are 10 to 600 nm particles in milk. When light run through the size of 10 nm particles, light will be scattered equally in front and rear direction. When light run through the size of 100 nm particles, light will be scattered to forward. “Forward” means the traveling direction of light. In other words, the experiment using milk is possible to create the turbidity environment that considers the various light scattering. In [12], the maximum amount of milk 1.9×10^2 ml/m^3 have been added. In [13], the maximum amount of milk 1.5×10^2 ml/m^3 have been added. Those researches described the monocular image recognition. There is no discussion on pose estimation using the dual eye cameras. In this study, the pose recognizable range using dual eye cameras on different turbidity and using active/passive 3D marker was analyzed. Finally, the experimental results show that the superiority of using the active 3D marker.

In the recognition experiment by using active 3D marker, maximum 2.45×10^2 ml/m^3 milk have been added. One times increase milk by 2.435 ml/m^3(2g) between 0 and 3.64×10 ml/m^3, 4.870 ml/m^3(4g) between 3.64×10 and 1.19×10^2 ml/m^3 and 9.740 ml/m^3(8g) between 1.19×10^2 and 2.45×10^2 ml/m^3.

C. Light Environment

The recognition experiment by using active 3D marker. The active 3D marker was used in the recognition experiment. According to the previous experiments [14], the red LED is set to 5.7 mA, green LED is set to 3.4 mA and red LED is set to 3.4 mA.

D. Comparison Method of Recognition Result

For the evaluation of recognition performance on different turbidity environments, the fitness value is used to evaluate the correlation between the 3D marker and 3D search model. The recognition level is evaluated by using the average of the fitness value between 60s from the start of recognition. Based on the average of the fitness value, setting Area I is defined as dockable range. Area II is recognizable range that means dockable but not as reliable as Area I. Area III is unrecognizable range. In the experiments, the superiority is compared by the size of the recognizable range.

V. Recognition experiments

In the recognition experiment by using active 3D marker, turbidity levels were divided into 46 parts from 0 to 2.45×10^2 ml/m^3. And, the distance between the ROV and 3D marker divided into 4 parts from 400 to 1000 mm. The total of 184 (= 46×4) recognition experiments were conducted. The amount of milk added each time is same as the experiment by using passive 3D marker. The reason for why it has different range of turbidly environment between active and passive 3D marker is that the recognition ability by using active 3D marker is possibly better than using passive 3D marker. When the distance between the ROV and the active 3D marker is 400 mm, it is the maximum turbidity that active 3D marker can be recognized.

The results of recognition experiments by using active 3D markers are shown in Table I. The amount of milk put into the pool is shown in the first column. The second to fifth columns show the average of the fitness value on each turbidity level when the distances from the ROV to active 3D marker are 400, 600, 800 and 1000 mm. In Table I, Area I represents the docking available area ($F \geq 0.60$). Area II represents the recognizable area ($0.22 \leq F < 0.60$). The remaining area(Area III), represents that the 3D marker cannot be detected by the RM-GA ($F < 0.22$). All the fitness value in the table is the average of the fitness value obtained from the recognition experiment of 60 seconds. In Fig. 4, real-time and average fitness values under the conditions designated by (A) in Table I are calculated by averaging above real-time measurement result Fig. 4(a), and (B) and (C) in Table I are calculated by Fig. 4(b) and (c).

Left and right camera images of the ROV in the areas I to III are shown in Fig. 5. The dotted line in the image shows the pose of the 3D search model. In the images of area I and II, it can be confirmed that the 3D search model converges to the 3D marker. However, in the Area III, the 3D search model cannot converge to the 3D marker. It can be confirmed that the result of the pose measurement of RM-GA is not correct.

In the previous work [15], the recognition experiments by using passive 3D marker have been performed. The experimental results are shown in Table II. When the docking experiments was conducted by using passive 3D marker, the visual servoing was performed from the 600 mm between the 3D marker and the ROV. By comparing the range of Area I in Table I and Table II, it can be confirmed that the result of docking available and recognizable ranges of active 3D marker are larger than that of passive 3D marker. In this way, the

TABLE I
THE EXPERIMENTAL RESULTS BY USING ACTIVE 3D MARKER

Milk ml/m^3(FTU) \ Distance mm	400	600	800	1000	
0(0)	0.792(0.040)	(A) 0.777(0.042)	0.803(0.044)	0.829(0.052)	
2.43(0)	0.795(0.040)	0.863(0.043)	0.859(0.047)	0.802(0.051)	
4.85(0.57)	0.811(0.040)	0.885(0.043)	0.837(0.044)	0.770(0.045)	
7.28(0.77)	0.801(0.039)	0.929(0.038)	0.824(0.042)	0.797(0.045)	
9.70(1.03)	0.845(0.036)	0.847(0.038)	0.838(0.040)	0.776(0.047)	
1.21×10(1.2)	0.865(0.038)	0.932(0.037)	0.849(0.040)	0.786(0.042)	
1.46×10(1.6)	0.852(0.034)	0.917(0.039)	0.842(0.038)	0.767(0.042)	
1.70×10(1.77)	0.862(0.032)	0.931(0.034)	0.816(0.040)	0.722(0.044)	Area I
1.94×10(1.7)	0.854(0.032)	0.927(0.032)	0.818(0.039)	0.705(0.045)	
2.18×10(2.47)	0.854(0.031)	0.916(0.035)	0.806(0.038)	0.707(0.039)	
2.43×10(2.6)	0.85(0.033)	0.917(0.033)	0.781(0.041)	0.673(0.040)	
2.67×10(3.03)	0.841(0.032)	0.890(0.032)	0.765(0.039)	0.703(0.044)	
2.91×10(3.5)	0.830(0.030)	0.885(0.032)	0.772(0.037)	0.608(0.038)	
3.15×10(3.57)	0.817(0.031)	0.850(0.029)	0.750(0.037)	0.613(0.043)	
3.40×10(3.9)	0.816(0.029)	0.875(0.034)	0.783(0.034)	0.610(0.040)	
3.64×10(4.07)	0.803(0.028)	(B) 0.840(0.033)	0.781(0.031)	0.607(0.040)	
4.12×10(4.67)	0.814(0.031)	0.818(0.030)	0.744(0.035)	0.531(0.039)	
4.61×10(5.17)	0.798(0.030)	0.803(0.032)	0.687(0.034)	0.447(0.045)	
5.09×10(6.87)	0.799(0.031)	0.805(0.035)	0.628(0.038)	0.380(0.045)	Area II
5.58×10(7.47)	0.779(0.029)	0.780(0.034)	0.617(0.031)	0.314(0.046)	
6.06×10(8.03)	0.792(0.030)	0.762(0.033)	0.560(0.031)	0.197(0.049)	
6.55×10(8.67)	0.782(0.033)	0.741(0.034)	0.475(0.042)	0.168(0.043)	
7.03×10(9.17)	0.793(0.033)	0.724(0.027)	0.491(0.035)	0.171(0.040)	Area III
7.52×10(9.8)	0.786(0.031)	0.683(0.028)	0.423(0.043)	0.089(0.033)	
8.00×10(10.57)	0.763(0.031)	0.674(0.028)	0.452(0.040)	0.220(0.049)	
8.49×10(11.33)	0.756(0.032)	0.645(0.032)	0.403(0.039)	0.187(0.048)	
8.97×10(11.93)	0.732(0.033)	0.614(0.031)	0.345(0.041)	0.154(0.045)	
9.46×10(12.23)	0.719(0.031)	(C) 0.580(0.032)	0.244(0.028)	0.094(0.035)	
9.94×10(12.73)	0.706(0.032)	0.572(0.034)	0.251(0.043)	0.108(0.037)	
1.04×10^2(13.13)	0.703(0.033)	0.505(0.033)	0.218(0.039)	0.051(0.024)	
1.09×10^2(14.07)	0.674(0.032)	0.469(0.036)	0.163(0.036)	0.049(0.024)	
1.14×10^2(14.6)	0.670(0.033)	0.472(0.035)	0.167(0.037)	0.053(0.028)	
1.19×10^2(15.03)	0.653(0.034)	0.401(0.036)	0.142(0.036)	0.041(0.020)	
1.29×10^2(18.33)	0.625(0.034)	0.289(0.036)	0.108(0.037)	0.049(0.023)	
1.38×10^2(18.5)	0.563(0.033)	0.272(0.038)	0.065(0.028)	0.054(0.027)	
1.48×10^2(19.07)	0.552(0.033)	0.145(0.023)	0.070(0.031)	0.046(0.022)	
1.58×10^2(20.33)	0.524(0.033)	0.181(0.034)	0.065(0.031)	0.049(0.027)	
1.67×10^2(20.93)	0.471(0.032)	0.089(0.028)	0.049(0.025)	0.049(0.025)	
1.77×10^2(22.8)	0.387(0.030)	0.109(0.022)	0.052(0.025)	0.046(0.022)	
1.87×10^2(23.67)	0.428(0.040)	0.092(0.021)	0.050(0.027)	0.047(0.024)	
1.96×10^2(24.97)	0.508(0.031)	0.091(0.023)	0.053(0.027)	0.072(0.028)	
2.06×10^2(25.77)	0.236(0.021)	0.077(0.027)	0.073(0.033)	0.042(0.020)	
2.16×10^2(27.73)	0.218(0.024)	0.067(0.024)	0.052(0.027)	0.040(0.019)	
2.26×10^2(28.5)	0.198(0.025)	0.065(0.029)	0.034(0.019)	0.038(0.019)	
2.35×10^2(29.47)	0.168(0.027)	0.059(0.027)	0.049(0.024)	0.047(0.023)	
2.45×10^2(30.63)	0.167(0.025)	0.069(0.025)	0.045(0.024)	0.044(0.020)	

TABLE II
THE EXPERIMENTAL RESULTS BY USING PASSIVE 3D MARKER [15]

Milk ml/m^3(FTU) \ Distance mm	400	600	800	1000	
0(0)	0.687(0.048)	(A) 0.735(0.025)	0.781(0.045)	0.751(0.032)	Area I
2.43(0)	0.881(0.028)	0.892(0.022)	0.761(0.023)	0.751(0.031)	
4.85(0)	0.776(0.037)	0.838(0.028)	0.724(0.026)	0.592(0.031)	
7.28(0)	0.924(0.028)	0.823(0.031)	0.663(0.026)	0.559(0.035)	
9.70(0)	0.881(0.029)	0.749(0.028)	0.576(0.033)	0.422(0.041)	
1.21×10(0)	0.771(0.034)	0.746(0.029)	0.566(0.048)	0.491(0.051)	Area II
1.46×10(0)	0.749(0.036)	0.701(0.029)	0.674(0.038)	0.459(0.047)	
1.70×10(0)	0.712(0.028)	0.655(0.031)	0.530(0.033)	0.303(0.055)	
1.94×10(3.03)	0.702(0.029)	0.646(0.031)	0.538(0.039)	0.284(0.059)	
2.18×10(3.75)	0.674(0.025)	0.751(0.031)	0.329(0.034)	0.062(0.009)	
2.43×10(4)	0.691(0.027)	(B) 0.706(0.034)	0.397(0.044)	0.058(0.007)	
2.67×10(4.5)	0.679(0.029)	0.712(0.032)	0.325(0.033)	0.134(0.020)	
2.91×10(6.6)	0.685(0.030)	0.655(0.036)	0.381(0.050)	0.060(0.006)	
3.15×10(7.1)	0.670(0.030)	0.646(0.034)	0.298(0.034)	0.052(0.013)	
3.40×10(7.5)	0.671(0.031)	0.653(0.036)	0.215(0.035)	0.055(0.016)	
3.64×10(7.6)	0.651(0.031)	0.589(0.037)	0.258(0.038)	0.058(0.012)	Area III
4.12×10(7.9)	0.642(0.028)	0.595(0.038)	0.181(0.046)	0.185(0.046)	
4.61×10(8.7)	0.613(0.029)	0.584(0.038)	0.161(0.044)	0.059(0.012)	
5.09×10(9.3)	0.622(0.029)	0.529(0.044)	0.158(0.045)	0.056(0.015)	
5.58×10(10.5)	0.583(0.058)	0.294(0.039)	0.124(0.046)	0.136(0.056)	
6.06×10(11.2)	0.581(0.027)	0.216(0.039)	0.098(0.036)	0.153(0.038)	
6.55×10(12.2)	0.547(0.028)	(C) 0.262(0.056)	0.131(0.018)	0.119(0.039)	
7.03×10(13.3)	0.568(0.032)	0.087(0.016)	0.139(0.024)	0.168(0.034)	
7.52×10(14.3)	0.448(0.026)	0.217(0.027)	0.053(0.020)	0.060(0.010)	
8.00×10(15.3)	0.551(0.033)	0.152(0.025)	0.059(0.011)	0.155(0.032)	
8.49×10(17.1)	0.373(0.055)	0.117(0.015)	0.061(0.012)	0.167(0.034)	
8.97×10(18.3)	0.489(0.041)	0.146(0.032)	0.150(0.020)	0.149(0.036)	
9.46×10(20.4)	0.447(0.035)	0.118(0.049)	0.189(0.026)	0.226(0.028)	
9.94×10(21.4)	0.426(0.037)	0.156(0.023)	0.150(0.024)	0.146(0.023)	
1.04×10^2(23)	0.400(0.047)	0.149(0.027)	0.170(0.033)	0.061(0.013)	
1.09×10^2(24.2)	0.100(0.010)	0.126(0.047)	0.130(0.024)	0.143(0.057)	
1.14×10^2(26.4)	0.089(0.017)	0.161(0.033)	0.168(0.031)	0.172(0.048)	
1.19×10^2(27.8)	0.174(0.022)	0.093(0.025)	0.212(0.023)	0.218(0.026)	

active 3D marker can expand the visible space in turbid water as compared with the passive 3D marker.

VI. EXPERIMENT IN THE ACTUAL SEA

Figure 6 shows the block diagram of proposed system. Images from dual-eye camera installed on a ROV are sent to the PC. Real-time pose estimation using 3D model based matching method and real-time multi-step GA is implemented as software implementation in PC. Based on the error between the desired pose and estimated pose, 3D motion controller outputs control signals to control the thrusters of the vehicle. Interface unit is for image capturing and digital to analog converting between the vehicle and PC.

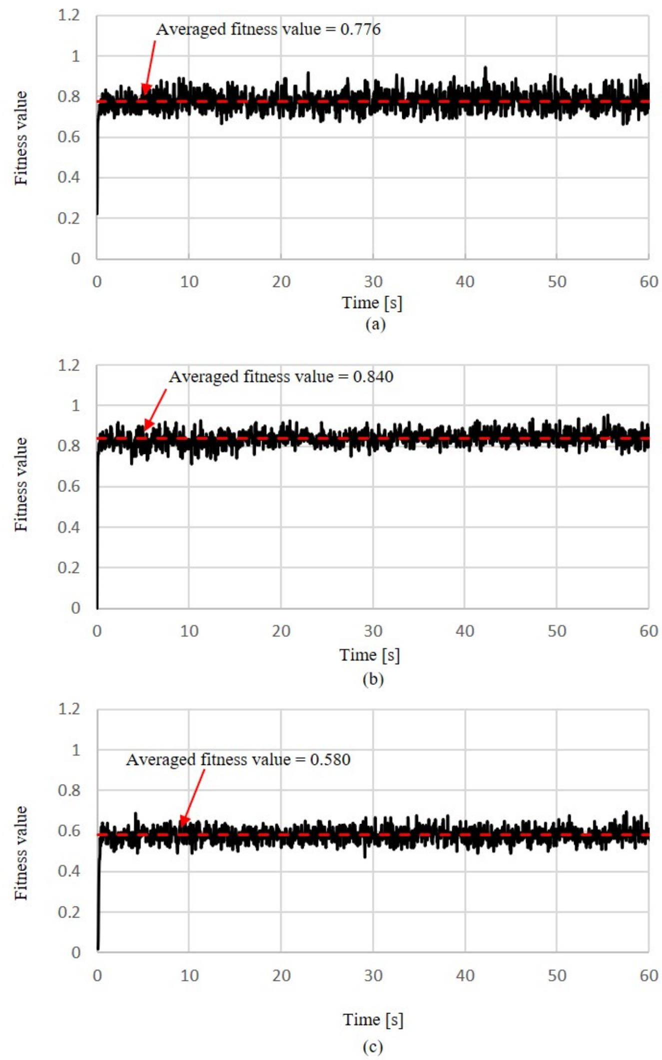

Fig. 4. Real-time and average fitness value 0.776 under the conditions designated by (A) in Table I is calculated by averaging above real-time measurement result (a), and (B) and (C) in Table I are calculated by above (b) and (c).

A. Underwater vehicle

Hovering type underwater vehicle (manufactured by Kowa cooperation) is used as a test bed as shown in Fig.7. Two fixed cameras installed at the front of the vehicle are used for real time pose tracking. In thruster unit, four thrusters with maximum thrust force of 4.9 each are controlled to move the vehicle along desired path. The vehicle can dive up to 50 m and two LED light sources are also installed on the vehicle.

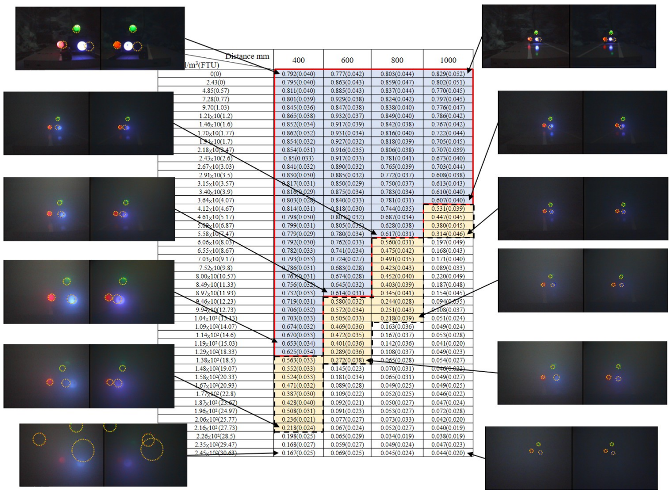

Fig. 5. Left and right camera images are taken under the turbidity conditions and considered distances, which are indicated by the arrow. Images taken at the maximum and minimum distances in clean water and at the maximum turbidity, in which the active 3D marker is not observable, are also shown at the top and bottom, respectively.

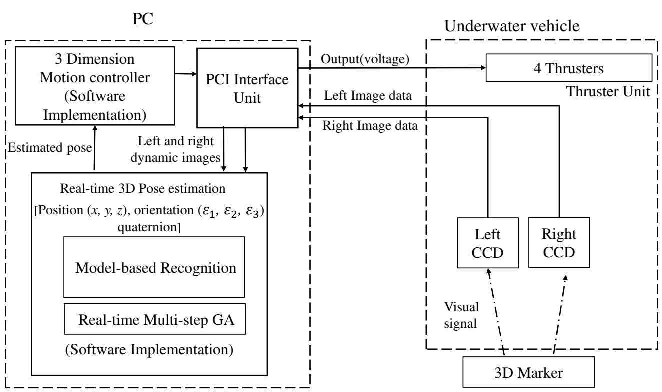

Fig. 6. Block diagram of the proposed System

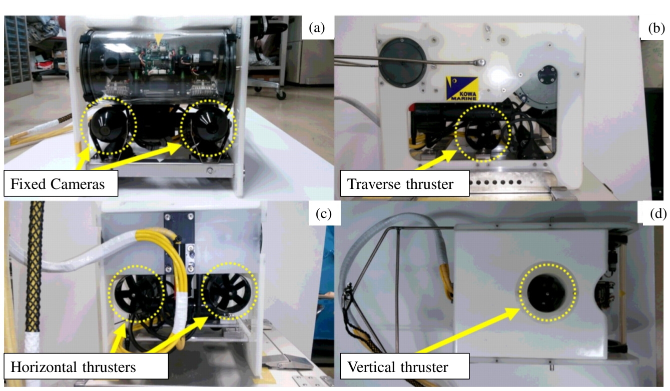

Fig. 7. Overview of ROV (a)Front view (b)Side view (c)Back view (d)Top view

B. Docking Procedure

We designed docking procedure as shown in Fig.8. There are three steps to complete docking operation.

(1) Approaching step: Normally, this step is performed using long distance navigation sensor unit. In this work, the vehicle was controlled by manually to approach the docking station till 3D marker was detected by proposed system.

(2) Visual servoing step: After detecting 3D marker, relative pose between the vehicle and 3D marker is estimated using 3D model-based matching method and real-time multi-step GA. Using estimated pose, the vehicle was controlled automatically using proposed system to follow the desired pose.

(3) Docking step: When the vehicle is stable in defined position for defined period for docking operation while visual servoing, docking step is performed in which the vehicle inserts its docking pole into the dock hole. Please note that whenever the relative pose error exceeds allowance range, the process switches to the visual servoing as shown as P in Fig.8.

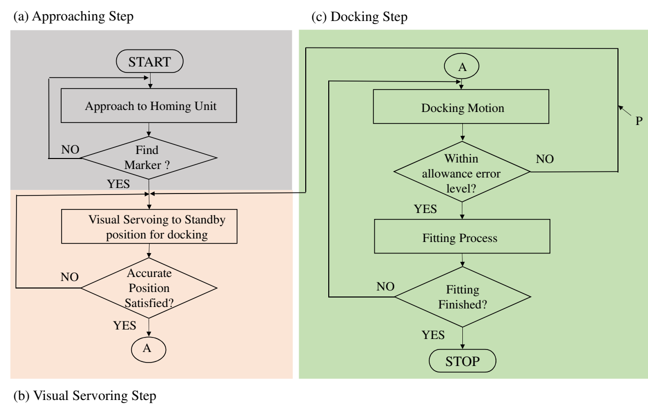

Fig. 8. Flowchart of Docking Strategy

C. Sea trial experiment

Our team conducted the sea docking trial experiment near Usimado city, in Japan for verifying the active 3D marker in the real sea environment. The docking station was a rectangle of 60 cm x 45 cm, oriented with the long sides perpendicular to the shore. The ROV was tethered and connected by a cable with 200 mm length to the onshore platform. For demonstration of underwater battery recharging, docking pole attached on vehicle and docking hole fixed with active 3D marker as shown in Fig.9 was designed. Therefore, the main task is to insert docking pole into the docking hole automatically controlling the vehicle by visual servoing. Firstly, the vehicle approached to the dock by manually until the 3D marker was in the field of view about 1.5 m distance. In visual servoing step, the vehicle goes to the desired pose for docking. When the vehicle is stable within desired pose, the vehicle goes ahead to insert decreasing the distance between vehicle and target in x-axis direction gradually until it reaches 350 mm.

D. Experimental results

We conducted docking operation successfully by using active 3D marker that originally failed in the same conditions

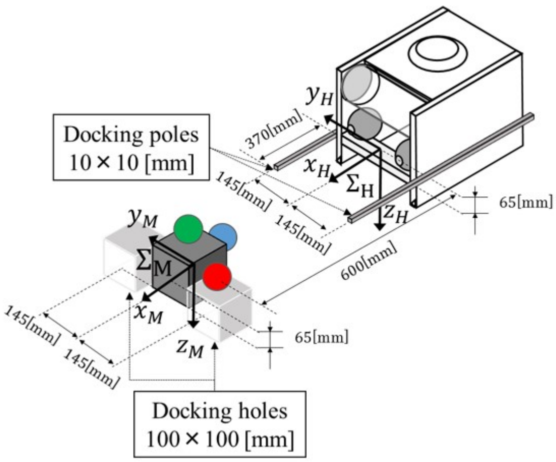

Fig. 9. Docking Experimental Layout

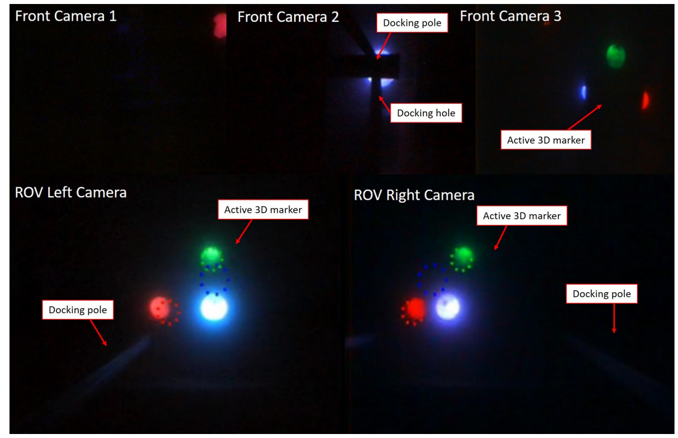

Fig. 11. Camera images added support line

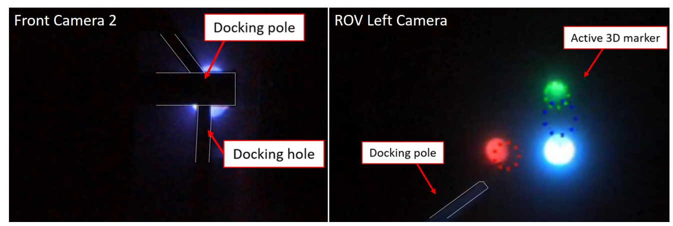

Fig. 12. Camera images add support line

by using passive 3D marker. Figure. 10 shows the fourth time trial docking experiment of the vehicle during docking process in the night time. Time profile of fitness value is shown in Fig. 10 (a). Recognized position of vehicle in x, y and z axis is illustrated in Fig. 10 (b)-(d). It can be seen that docking step was performed when the position errors in y-axis and z-axis were within predefined range that was ± 40 mm. It can be confirmed that the docking operation was success within 50s after recognition active 3D marker. Figure 11 shows the docking experiments in the night time. Figure 12 shows the overlay images in Front Camera 2 and ROV Left Camera of Fig. 12 for emphasizing the result of the docking. In this way, the active 3D marker enables ROV to perform docking to the station in the dark and turbid environment.

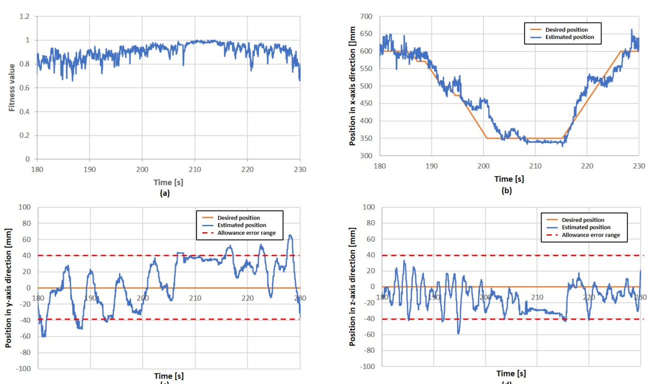

Fig. 10. Fourth time trial docking experiment

VII. Conclusion

In this study, an active 3D marker was proposed to overcome the problem of difficulty to recognize the target in the turbid environments. To confirm the effectiveness of the proposed active 3D marker, milk was put into the pool to create turbid environments. The recognition performance was compared between active and passive 3D marker. According to the experimental results, it can be confirmed that using the active 3D marker is more recognizable under the high turbidity environment than using passive 3D marker. In addition, the docking operation in actual sea by using active 3D marker is successful that originally failed in the same conditions by using passive 3D marker.

References

[1] Park, J-Y., Jun, B-H., Lee, P-M. and Oh, J., Experiments on vision guided docking of an autonomous underwater vehicle using one camera, Ocean Engineering, Vol. 36, No. 1 (2009), pp.48–61.

[2] Ura, T., Kurimoto, Y., Kondo, H., Nose, Y., Sakamaki, T. and Kuroda, Y., Observation behavior of an AUV for ship wreck investigation, Proceedings of the OCEANS 2005 MTS/IEEE, Vol. 3 (2005), pp.2686–2691.

[3] Ishii, K., Sonoda, T., Nakanishi, R., Kawashima, S. and Hidaka, S., Research on docking control of autonomous underwater vehicle, ROBOMECH2015 in Kyoto (2015), 2A2-D06 (in Japanese).

[4] Myo Myint, Kenta YONEMORI, Akira YANOU, Shintaro ISHIYAMA and Mamoru MINAMI. Robustness of Visual-Servo against Air Bubble Disturbance of Underwater Vehicle System Using Three-Dimensional Marker and Dual-Eye Cameras. Proceedings of the International Conference OCEANS15 MTS/IEEE. Washington DC, USA. pp.1-8. 2015.

[5] Myo Myint, Kenta Yonemori, Akira Yanou, Khin Nwe Lwin, Mamoru Minami and Shintaro Ishiyama. Visual Servoing for Underwater Vehicle Using Dual-eyes Evolutionary Real-time Pose Tracking. Journal of Robotics and Mechatronics. vol.28, no.4, pp.543-558. 2016.

[6] Myo Myint, Kenta Yonemori, Akira Yanou, Mamoru Minami and Shintaro Ishiyama. Visual-servobased Autonomous Docking System for Underwater Vehicle Using Dual-eyes Camera 3D-Pose Tracking. Proceedings of the 2015 IEEE/SICE International Symposium on System Integration. Nagoya, Japan. pp.989-994. 2015.

[7] Myo Myint, Kenta YONEMORI, Akira YANOU, Khin Nwe Lwin, Mamoru MINAMI and Shintaro ISHIYAMA. Visual-based Deep Sea Docking Simulation of Underwater Vehicle Using Dual-eyes Cameras with Lighting Adaptation. Proceedings of the International Conference OCEANS16 MTS/IEEE. Shanghai, China. pp.1-8. 2016.
[8] Kenta YONEMORI, Akira YANOU, Myo Myint, Khin Nwe Lwin, and Mamoru MINAMI. Docking experiment of underwater vehicle by dual-eye visual servoing in sea. Transactions of the JSME (in Japanese), Vol.83, No.848, 2017.
[9] Myo Myint, Khin Nwe Lwin, Naoki Mukada, Daiki Yamada, Takayuki Matsuno, Yuuichirou Yoda, Saitou Kazuhiro, Mamoru Minami, Experimental Verification of Turbidity Tolerance of Stereo-vision-based 3D Pose Estimation System, Journal of Marine Science and Technology, DOI 10.1007/s00773-018-0586-7, 2018 (24 pages).
[10] Khin Nwe Lwin, Naoki Mukada, Myo Myint, Daiki Yamada, Akira Yanou, Takayuki Matsuno, Kazuhiro Saitou, Waichiro Godou, Tatsuya Sakamoto, Mamoru Minami, "Visual Docking against Bubble Noise with Three-dimensional Perception Using Dual-eye Cameras", IEEE Journal of Oceanic Engineering
[11] Myo, M., Kenta Y., Khin N. L., Akira Y. and Mamoru M., Dual-eyes Vision-based Docking System for Autonomous Underwater Vehicle: an Approach and Experiments, Journal of Intelligent and Robotic Systems (2017b), DOI:10.1007/s10846-017-0703-6.
[12] Garcia, R. and Gracias, N., Detection of interest points in turbid underwater images, In OCEANS, 2011 IEEE-Spain (2011), pp.1–9.
[13] Codevilla, F., Gaya, J.D.O., Duarte, N. and Botelho, S., Achieving turbidity robustness on underwater images local feature detection, International journal of computer vision (2004), 60 (2), pp.91–110.
[14] Yoshiki Kanda, Naoki Mukada, Daiki Yamada, Khin Lwin, Myo Myint, Kohei Yamashita, Sho Nakamura, Takayuki Matsuno, Mamoru Minami, "Development and Evaluation of Active/Lighting Marker in Turbidity and Illumination Variation Environments," Proceedings of IEEE/MTS Techno-Ocean Conference 2018, Paper No.171129-095, Kobe, Japan, May 29-31,2018
[15] Horng-Yi Hsu, Naoki Mukada, Daiki Yamada, Khin Nwe Lwin, Myo Myint, Yuichiro Toda, Takayuki Matsuno, Keigo Watanabe, and Mamoru Minami, "Stereo-vision visibility analyses in relation with turbidity and distance for AUV recharge docking," 24th International Symposium on Artificial Life and Robotics, B-Con PLAZA, Beppu, JAPAN, pp.905-910, January 23-25, 2019